

MINI-GEMINI: MINING THE POTENTIAL OF MULTI-MODALITY VISION LANGUAGE MODELS

Anonymous authors

Paper under double-blind review

ABSTRACT

In this work, we introduce Mini-Gemini, a simple and effective framework enhancing multi-modality Vision Language Models (VLMs). Despite the advancements in VLMs facilitating basic visual dialog and reasoning, a performance gap persists compared to advanced models like GPT-4 and Gemini. We try to narrow the gap by mining the potential of VLMs for better performance across various cross-modal tasks from three aspects, *i.e.*, high-resolution visual tokens, high-quality data, and VLM-guided generation. To enhance visual tokens, we propose to utilize an additional visual encoder for high-resolution refinement without increasing the visual token count. We further construct a high-quality dataset that promotes precise image comprehension and reasoning-based generation, expanding the operational scope of current VLMs. In general, Mini-Gemini further mines the potential of VLMs and empowers current frameworks with image understanding, reasoning, and generation simultaneously. Mini-Gemini supports a series of dense and MoE Large Language Models (LLMs) from 2B to 34B. It is demonstrated to achieve leading performance in several zero-shot benchmarks and even surpasses the developed private models. Code and models will be available to the public.

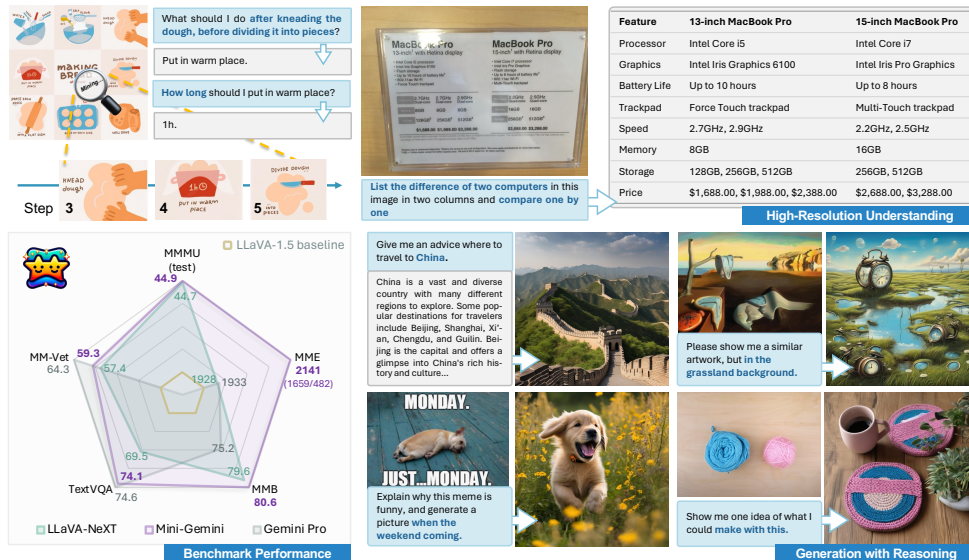


Figure 1: Mini-Gemini is advanced in various vision-related tasks.

1 INTRODUCTION

With the rapid evolution in Large Language Models (LLMs) OpenAI (2023a); Zhang et al. (2022); Touvron et al. (2023), empowering the impressive capabilities for multi-modality inputs is becoming an essential part of current Vision Language Models (VLMs) OpenAI (2023b); Team et al. (2023). To bridge the modality gap, several studies are conducted to marry vision with LLMs from images Li et al. (2023c); Liu et al. (2023b); Zhu et al. (2023) to videos Zhang et al. (2023a); Li et al. (2023d). Despite these advancements, a significant gap remains between academic initiatives and the prowess

of well-established models like GPT-4 [OpenAI \(2023b\)](#) and Gemini [Team et al. \(2023\)](#), which are trained with huge amounts of data and resources.

For vision itself, image resolution is a core part of explicitly despite the surrounding environment with minimal visual hallucination. To this end, more attempts are performed to further improve the visual understanding in current VLMs. For instance, SPHINX [Lin et al. \(2023\)](#), Otter-HD [Li et al. \(2023a\)](#), and LLaVA-Next [Liu et al. \(2024\)](#) are proposed to enhance the ability based on previous work [Dai et al. \(2023\)](#); [Liu et al. \(2023b\)](#); [Bavishi et al. \(2023\)](#) by improving the image resolution. Increasing the number of visual tokens with higher-resolution images undeniably enriches visual embeddings in LLMs. However, this improvement comes with escalated computational demands and associated costs, particularly when processing multiple images. Moreover, the existing data quality, model capabilities, and application scopes remain inadequate for accelerated training and development processes. This scenario prompts a critical inquiry: *how to push forward the VLMs approaching well-developed models with acceptable cost in an academic setting?*

To answer this question, we explore the potential of VLMs from three strategic aspects, *i.e.*, efficient high-resolution solution, high-quality data, and expanded applications. Firstly, we utilize ConvNet to efficiently generate higher-resolution candidates, thus enhancing visual detail while maintaining the visual token count for LLMs. To bolster data quality, we amalgamate high-quality datasets from diverse public sources, ensuring a rich and varied data foundation. Furthermore, our approach integrates these enhancements with cutting-edge LLMs and generative models, aiming to elevate VLM performance and user experience. This multifaceted strategy enables us to delve deeper into the capabilities of VLMs, achieving significant advancements within manageable resource constraints.

In general, our method is adept at handling both image and text as input and output. In particular, we introduce an efficient visual token enhancement pipeline for input images, featuring a dual-encoder system. It comprises twin encoders, one for high-resolution images and the other for low-resolution visual embedding, mirroring the cooperative functionality of the Gemini constellation. During inference, they work in an attention mechanism, where the low-resolution one generates visual queries, and the high-resolution counterpart provides candidate keys and values for reference. To augment the data quality, we collect and produce more data based on public resources, including high-quality responses [Chen et al. \(2023b; 2024\)](#), task-oriented instructions [Goyal et al. \(2017\)](#); [Tito et al. \(2021\)](#); [Masry et al. \(2022\)](#); [Kembhavi et al. \(2016\)](#), and generation-related data [Zhou et al. \(2024\)](#); [Köpf et al. \(2024\)](#). The increased amount and quality improve the overall performance and extend the capability of model. Additionally, our model supports concurrent image and text generation, facilitated by the seamless integration of our VLM with advanced generative models [Podell et al. \(2023\)](#). It leverages VLM guidance for image generation by providing the generated text from LLMs.

The Mini-Gemini framework, can be easily instantiated with a range of LLMs from 2B to 34B parameter scales, as detailed elaborated in Section 3. Extensive empirical studies are conducted in Section 4 to reveal the effectiveness of the proposed method. Remarkably, our approach attains leading performance in various settings and even surpasses the well-developed Gemini Pro [Team et al. \(2023\)](#), Qwen-VL-Plus [Bai et al. \(2023\)](#), and GPT 4V [OpenAI \(2023b\)](#) in the complex MMB [Liu et al. \(2023c\)](#) and MMU [Yue et al. \(2024\)](#) dataset, respectively. These results underscore Mini-Gemini’s potential to set new benchmarks in the realm of VLMs, highlighting its advanced capabilities in handling complex multi-modal tasks.

2 RELATED WORK

Large Language Models. Recent progress in Natural Language Processing (NLP) has been dramatically accelerated by advancements in large language models (LLMs). The seminal introduction of the Transformer framework [Vaswani et al. \(2017\)](#) served as a cornerstone, enabling a new wave of language models [Devlin et al. \(2018\)](#); [Zhang et al. \(2022\)](#). The inception of the Generative Pre-trained Transformer (GPT) [Brown et al. \(2020\)](#) introduced a novel paradigm through auto-regressive language modeling, establishing a robust method for language prediction and generation. The emergence of models [OpenAI \(2023a;b\)](#); [Touvron et al. \(2023\)](#); [Jiang et al. \(2024\)](#) further exemplified the field’s rapid evolution, each demonstrating enhanced performance on complex language processing tasks. Instruction tuning [Wei et al. \(2021\)](#); [Ouyang et al. \(2022\)](#) has emerged as a key technique for refining the output of pre-trained LLMs, as evidenced by its application in the development of open-source models [Taori et al. \(2023\)](#); [Chiang et al. \(2023\)](#). They iterate on the LLaMA [Touvron et al. \(2023\)](#) with custom instruction sets. Additionally, the integration of LLMs with specific tools for visual

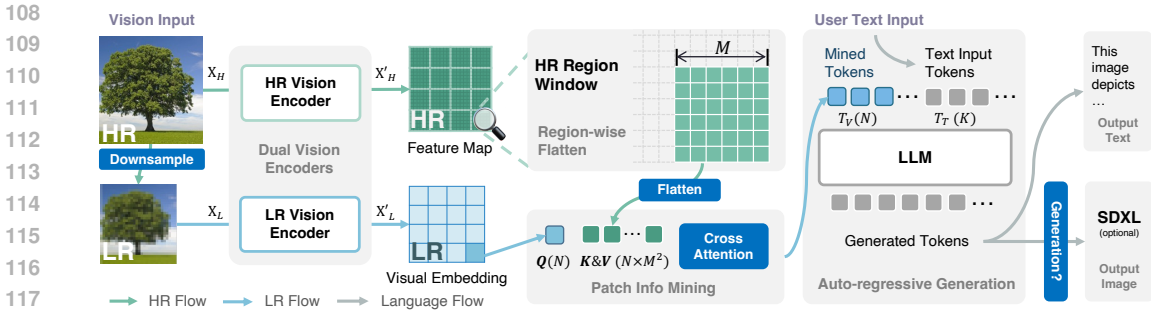


Figure 2: The framework of Mini-Gemini’s workflow.

tasks [Wu et al. \(2023a\)](#); [Yang et al. \(2023\)](#) highlights their adaptability and potential for broad application, underscoring the utility of LLMs in extending beyond traditional text-based processing to include multimodal interactions. In this work, we take several pre-trained LLMs [Google \(2024\)](#); [Touvron et al. \(2023\)](#); [Jiang et al. \(2024\)](#) as benchmarks and build multi-modality frameworks upon them to further extend the impressive reasoning ability.

Vision Language Models. The convergence of different modalities has given rise to VLMs. This integration has been pivotal in advancing tasks that require both visual understanding and language processing, as evidenced by models trained on diverse datasets for understanding [Chen et al. \(2015\)](#) and reasoning [Goyal et al. \(2017\)](#); [Lu et al. \(2022\)](#); [Lai et al. \(2023\)](#). Groundbreaking models such as CLIP [Radford et al. \(2021\)](#) have further bridged the gap between language models and vision tasks. Recent developments underscore a growing trend toward leveraging the robust capabilities of LLMs within the realm of VLMs. Innovations like Flamingo [Alayrac et al. \(2022\)](#) and BLIP-2 [Li et al. \(2023c\)](#) have capitalized on massive collections of image-text pairs to fine-tune cross-modal alignment, significantly boosting learning efficiency. Building upon these advancements, several models [Dai et al. \(2023\)](#); [Zhu et al. \(2023\)](#) have focused on generating high-quality instructional data based on BLIP-2, leading to marked improvements in performance. Furthermore, LLaVA [Liu et al. \(2023b;a\)](#) adopts a simple linear projector to facilitate image-text space alignment with minimal learnable parameters. It leverages tailored instruction data and exemplifies an efficient strategy that demonstrates the model’s potent capabilities. Different from them, we aim to explore the potential for both comprehension and generation.

LLM as Generation Assistant. Combining LLMs with image outputs has emerged as a pivotal area in recent multimodal research. Methods like InternLM-XComposer [Zhang et al. \(2023b\)](#); [Dong et al. \(2024\)](#) utilize image retrieval to produce interleaved text and image outputs, bypassing direct generation. Conversely, auto-regressive token prediction approaches, exemplified by EMU [Sun et al. \(2023b;a\)](#) and SEED [Ge et al. \(2023a;b\)](#), enable LLMs to decode images through massive image-text data directly. These methods require enormous training resources, and their auto-regressive nature leads to undesirable latency. Recent studies [Xia et al. \(2023\)](#); [Chi et al. \(2023\)](#); [Zhan et al. \(2024\)](#) strive to align with latent diffusion models [Podell et al. \(2023\)](#) to streamline image generation. They typically require designing text embeddings and additional optimization to achieve the desired generation effect. This joint training can compromise the performance of VLMs in text generation. Mini-Gemini distinguishes itself by adopting a text-data-driven approach to enable the model to generate high-quality images. We leverage a mere 13K pure text data to activate the LLM’s ability as a high-quality re-captioner [Betker et al. \(2023\)](#) without undermining the fundamental performance of VLMs.

3 MINI-GEMINI

The framework of Mini-Gemini is conceptually simple: dual vision encoders are utilized to provide low-resolution visual embedding and high-resolution candidates; patch info mining is proposed to conduct patch-level mining between high-resolution regions and low-resolution visual queries; LLM is utilized to marry text with images for both comprehension and generation at the same time.

3.1 DUAL VISION ENCODERS

In the Mini-Gemini framework, both text and image inputs can be processed, with the option to handle them individually or in combination. For illustrative clarity, we consider the concurrent processing

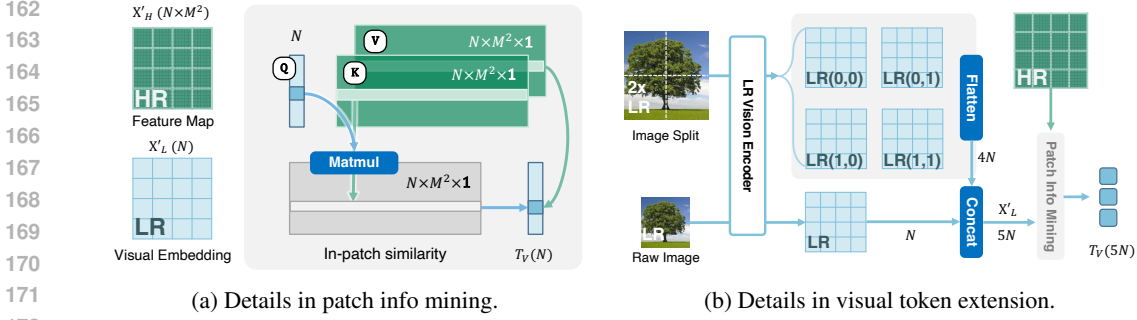


Figure 3: More details in patch info mining and visual token extension.

of both modalities. As depicted in Figure 2, the processing begins with a high-resolution image $X_H \in \mathbb{R}^{H \times W \times 3}$, from which a corresponding low-resolution image $X_L \in \mathbb{R}^{H' \times W' \times 3}$ is generated via bilinear interpolation, ensuring $H' \leq H$. Then, we process them and encode into multi-grid visual embeddings in two parallel image flows. In particular, for the low-resolution (LR) flow, we maintain the traditional pipeline Dai et al. (2023); Liu et al. (2023b) and employ a CLIP-pretrained ViT Radford et al. (2021) to encode the visual embedding $X'_L \in \mathbb{R}^{N \times C}$, where N denotes the number of visual patches. In this way, the long-range relation among N visual patches can be well preserved for subsequent interaction in LLMs. As for the high-resolution (HR) flow, we adopt the CNN-based encoder for adaptive and efficient HR image processing. For instance, to align with the LR visual embedding, the LAION-pretrained Schuhmann et al. (2022) ConvNeXt Liu et al. (2022) is used to serve as an HR vision encoder. Therefore, we can obtain the HR feature map $X'_H \in \mathbb{R}^{N' \times C}$ by upsampling and concatenating the features from different convolutional stages to 1/4 input scale. Here, $N' = H/4 \times W/4 = N \times M^2$ denotes the number of HR features, where M reflects the pixel-wise feature count within each HR segment, as illustrated in Figure 2.

3.2 PATCH INFO MINING

With the above generated LR embedding X'_L and HR feature X'_H , we propose patch info mining to extend the potential of VLMs with enhanced visual tokens. In particular, to maintain the number of final visual tokens for efficiency in LLMs, we take the low-resolution visual embedding X'_L as query $Q \in \mathbb{R}^{N \times C}$, aiming to retrieve relevant visual cues from HR candidate. Meanwhile, the HR feature map X'_H is taken as key $K \in \mathbb{R}^{N \times M^2 \times C}$ and value $V \in \mathbb{R}^{N \times M^2 \times C}$, as depicted in Figure 2. Here, the low-resolution patch in Q correlates with a corresponding high-resolution sub-region in K and V , encompassing M^2 pixel-wise features. Therefore, the patch info mining process can be formulated as

$$T_V = \text{MLP}(Q + \text{Softmax}(\phi(Q) \times \phi(K)^T) \times \phi(V)), \quad (1)$$

where ϕ and MLP indicate a projection layer and a multi-layer perceptron, respectively. As presented in Figure 3a, this formula encapsulates the process of synthesizing and refining the visual cues, leading to generation of enhanced visual tokens T_V for subsequent LLM processing. It ensures that the mining for each query is confined to its corresponding sub-region in X'_H with M^2 features, thus preserving efficiency. This design allows for the extraction of HR details without expanding the visual token count of T_V , maintaining a balance between richness of detail and computational feasibility.

Furthermore, visual token extension is also supported in the designed patch info mining. As depicted in Figure 3b, we can extend the visual token to $5N$ to capture more details. This is achieved by incorporating the original image along with its $2 \times$ upscaled counterpart, resulting in a batched input $X_L \in \mathbb{R}^{5 \times H' \times W' \times 3}$. And we can get the encoded visual embedding $X'_L \in \mathbb{R}^{5 \times N \times C}$ with the LR vision encoder, as detailed in Section 3.1. Thanks to the flexible design of CNN-based HR vision encoder, it can adeptly handle the augmented visual token count during the patch info mining. The only difference in the aforementioned procedure is the sub-region in X'_H should be changed according to the expanded visual embedding X'_L . We can also upsample the HR input to better support the higher resolution if needed, as experimentally analyzed in Table 4.

3.3 TEXT AND IMAGE GENERATION

With the mined visual tokens T_V and input text tokens T_T , we concatenate them as the input to LLMs for auto-regressive generation, as presented in Figure 2. Distinguished from traditional VLMs Dai

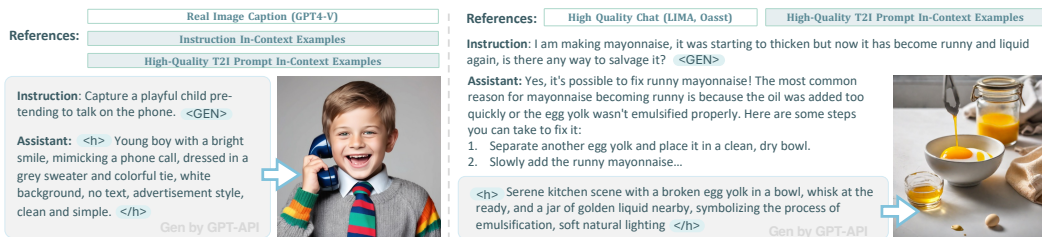


Figure 4: Two types of our pure-text data are used for image generation. *Left*: Simple instruction re-caption and *Right*: In-context prompt generation. SDXL generates images with the output prompt.

et al. (2023); Liu et al. (2023a; 2024), the proposed Mini-Gemini supports both text-only and text-image generation as input and output. Despite the image comprehension, we anchor Mini-Gemini’s ability to generate images on its outstanding image-text understanding and reasoning capabilities. Unlike recent works Xia et al. (2023); Chi et al. (2023); Zhan et al. (2024); Sun et al. (2023a); Aiello et al. (2023), which address the domain gap between text embeddings of LLMs and generation models, we choose to optimize the gap in the domain of language prompts. Precisely, Mini-Gemini translates user instructions into high-quality prompts that produce context-relevant images in latent diffusion models Podell et al. (2023); Pernias et al. (2023). This approach is reflected in subsequent high-quality image generation frameworks, such as DALLE 3 Betker et al. (2023) and SORA OpenAI, which leverage the generation and understanding capabilities of VLMs to obtain higher-quality text conditions for generation tasks.

Text-image Instructions. For better cross-modality alignment and instruction finetuning, we collect high-quality datasets from publicly available sources. In particular, for cross-modality alignment, we utilize 558K image-caption pairs from the LLaVA-filtered CC3M dataset Sharma et al. (2018) and 695K sampled GPT-4V-responded captions from the ALLaVA dataset Chen et al. (2024). It brings about 1.2M image captions in total for projector pretraining. As for instruction finetuning, we sample 643K single- and multi-turn conversations (excluding 21K TextCaps Sidorov et al. (2020) data) from the LLaVA Liu et al. (2023a) dataset, 100K QA pairs from ShareGPT4V Chen et al. (2023b), 10K LAION-GPT-4V eV captions, 700K GPT-4V-responded instruction pairs from ALLaVA dataset Chen et al. (2024), and 6K text-only multi-turn conversations from LIMA Zhou et al. (2024) and OpenAssistant2 Köpf et al. (2024). To bolster the OCR-related abilities, we further collect 28K QA pairs that comprise 10K DocVQA Tito et al. (2021), 4K ChartQA Masry et al. (2022), 10K DVQA Kafle et al. (2018), and 4K AI2D Kembhavi et al. (2016) data. In general, there are about 1.5M instruction-related conversations for image comprehension. Moreover, we also collect 13K pairs for image-related generation that will be elaborated on subsequently.

Generation-related Instructions. To support image generation, we further construct a 13K instruction-following dataset using GPT-4 Turbo. As depicted in Figure 4, the training data encompasses two tasks: (a) Simple instruction re-caption: we adopt 8K descriptive image captions from LAION-GPT-4V eV and let GPT-4 inversely infer the corresponding user’s short input and the target caption in the Stable Diffusion (SD) domain. (b) In-context prompt generation: based on a few high-quality real-world conversation contexts in LIMA Zhou et al. (2024) and OpenAssistant2 Köpf et al. (2024), we generate prompts that produce images suitable for the conversation context, bringing 5K instructions in total. For both kinds of data, in each query to GPT-4, we randomly sample 5 high-quality SD text-to-image prompts from GigaSheet Gig as in-context examples to obtain target prompts for generation. We format our data to use <GEN> as a trigger to initiate the generation process and wrap the target caption within <h> . . . </h>. Following text generation, Mini-Gemini extracts target captions and utilizes SDXL Podell et al. (2023) to generate the corresponding image. More details are discussed in Appendix B.

4 EXPERIMENTS

4.1 EXPERIMENTAL SETUP

Implementation Details. In this study, we instantiate Mini-Gemini with the CLIP-pretrained ViT-L Radford et al. (2021) for LR vision encoder and the LAION-pretrained ConvNeXt-L Schuhmann et al. (2022) for HR vision encoder. For efficient training, we keep two vision encoders fixed and optimize the projectors of patch info mining in all stages. Meanwhile, we optimize the LLM during

Table 1: Comparison with leading methods on zero-shot benchmarks. * and † denote images in *train* subset are included and the data is not publicly available, respectively. Our results are marked with **.**

Method	LLM	Res.	VQA ^T	MMB	MME	MM-Vet	MMMU _v	MMMU _t	MathVista
<i>Normal resolution setting</i>									
MobileVLM Chu et al. (2023)	MLLaMA 2.7B	336	47.5	59.6	1289	–	–	–	–
InstructBLIP Dai et al. (2023)	Vicuna-7B	224	50.1	36.0	–	26.2	–	–	25.3
InstructBLIP Dai et al. (2023)	Vicuna-13B	224	50.7	–	1213	25.6	–	–	–
Qwen-VL† Bai et al. (2023)	Qwen-7B	448	63.8*	38.2	–	–	–	–	–
Qwen-VL-Chat† Bai et al. (2023)	Qwen-7B	448	61.5*	60.6	1488	–	35.9	32.9	–
Shikra Chen et al. (2023a)	Vicuna-13B	224	–	58.8	–	–	–	–	–
IDEFICS-80B IDEFICS (2023)	LLaMA-65B	224	30.9	54.5	–	–	–	–	–
LLaMA-VID Li et al. (2023d)	Vicuna-7B	336	–	65.1	1521	–	–	–	–
LLaMA-VID Li et al. (2023d)	Vicuna-13B	336	–	66.6	1542	–	–	–	–
LLaVA-1.5 Liu et al. (2023a)	Vicuna-7B	336	58.2	65.2	1511	31.1	–	–	–
LLaVA-1.5 Liu et al. (2023a)	Vicuna-13B	336	61.3	69.2	1531/295	36.1	36.4	33.6	27.6
Mini-Gemini	Gemma-2B	336	56.2	59.8	1341/312	31.1	31.7	29.1	29.4
Mini-Gemini	Vicuna-7B	336	65.2	69.3	1523/316	40.8	36.1	32.8	31.4
Mini-Gemini	Vicuna-13B	336	65.9	68.5	1565/322	<u>46.0</u>	38.1	33.5	37.0
Mini-Gemini	Mixtral-8x7B	336	<u>69.2</u>	<u>75.6</u>	<u>1639/379</u>	45.8	<u>41.8</u>	<u>37.1</u>	41.8
Mini-Gemini	Hermes-2-Yi-34B	336	70.1	79.6	1666/439	53.0	48.7	43.6	<u>38.9</u>
<i>High resolution setting</i>									
OtterHD Li et al. (2023a)	Fuyu-8B	1024	–	53.6	1314	–	–	–	–
CogVLM-Chat Wang et al. (2023)	Vicuna-7B	490	70.4*	63.7	–	51.1	41.1	–	34.5
LLaVA-NeXT Liu et al. (2024)	Vicuna-7B	672	64.9	68.1	1519/332	43.9	35.8	–	34.6
LLaVA-NeXT Liu et al. (2024)	Vicuna-13B	672	67.1	70.7	1575/326	48.4	36.2	–	35.3
LLaVA-NeXT Liu et al. (2024)	Hermes-2-Yi-34B	672	69.5	<u>79.6</u>	<u>1631/397</u>	<u>57.4</u>	51.1	<u>44.7</u>	46.5
Mini-Gemini-HD	Vicuna-7B	672	68.4	65.8	1546/319	41.3	36.8	32.9	32.2
Mini-Gemini-HD	Vicuna-13B	672	70.2	68.6	1597/320	50.5	37.3	35.1	37.0
Mini-Gemini-HD	Mixtral-8x7B	672	<u>71.9</u>	<u>74.7</u>	<u>1633/356</u>	53.5	40.0	37.0	43.1
Mini-Gemini-HD	Hermes-2-Yi-34B	672	74.1	80.6	1659/482	59.3	<u>48.0</u>	44.9	<u>43.3</u>
<i>Private models</i>									
Gemini Pro Team et al. (2023)	Private	–	74.6	75.2	–	64.3	47.9	–	45.2
Qwen-VL-Plus Bai et al. (2023)	Private	–	78.9	66.2	–	–	45.2	40.8	43.3
GPT-4V OpenAI (2023b)	Private	–	78.0	75.1	–	67.6	56.8	55.7	49.9

the instruction tuning stage only. Regarding the training scheme, we optimize all the models for 1 epoch with the AdamW optimizer and a Cosine learning schedule. In most cases, the initial learning rates for modality alignment and instruction tuning are respectively set at $1e^{-3}$ and $2e^{-5}$, with an adjusted rate of $1e^{-5}$ for the Mixtral-8×7B and Hermes-2-Yi-34B to ensure stable instruction tuning. The framework involves training on 8×A800 GPUs for standard machine configurations. For the largest model with Hermes-2-Yi-34B, we leverage 4 machines and complete the optimization within 2 days with DeepSpeed Zero3 strategy. For the HD version, the total cost is enlarged to about 4 days because of the extended visual tokens in LLMs.

Datasets. For model optimization, we construct high-quality data for cross-modality understanding and generation. It mainly includes 1.2M caption pairs for modality alignment and 1.5M single- or multi-round conversations for instruction tuning, as elaborated in Section 3.3. Moreover, we report results on widely-adopted zero-shot image-based benchmarks, including VQA^T (TextVQA) [Singh et al. \(2019\)](#), MMB (MMBench) [Liu et al. \(2023c\)](#), MME [Fu et al. \(2023\)](#), MM-Vet [Yu et al. \(2023\)](#), MMMU [Yue et al. \(2024\)](#), and MathVista [Lu et al. \(2024\)](#) datasets.

4.2 MAIN RESULTS

Normal Resolution. In Table 1, we compare with previous leading approaches across several settings, including normal and high resolution, and also consider private models. At normal resolution, Mini-Gemini consistently outperforms existing models across a wide range of LLMs. In the efficient model category, Mini-Gemini, when configured with Gemma-2B [Google \(2024\)](#), demonstrates superior performance compared to the efficient MobileVLM [Chu et al. \(2023\)](#) and even surpasses InstructBLIP [Dai et al. \(2023\)](#) equipped with Vicuna-7B and even 13B. The scalability of Mini-Gemini is evident when larger LLMs are employed. Given the same LLM, the proposed Mini-Gemini is validated to surpass LLaVA-1.5 [Liu et al. \(2023a\)](#) with a large margin across all benchmarks. Notably, with the Hermes-2-Yi-34B LLM, Mini-Gemini achieves exceptional results, outpacing high-resource private models like Qwen-VL-Plus [Bai et al. \(2023\)](#) and Gemini Pro [Team et al. \(2023\)](#) in some challenging benchmarks like MMMU [Yue et al. \(2024\)](#) and MMB [Liu et al. \(2023c\)](#).

Table 2: Comparison of different methods with their latency breakdown. All methods use Vicuna-7B.

Method	Res.	LR Encoder	HR Encoder	Patch Info Mining	LLM	Total (ms)	TFLOPS (100 tokens)
LLaVA-1.5	336	10.6	–	–	3318.3	3328.9	5.0
LLaVA-NeXT	672	25.3	–	–	6062.6	6087.9	21.2
Mini-Gemini	336	10.5	15.5	4.8	3913.7	3944.5	5.5
Mini-Gemini-HD	672	25.5	52.1	28.7	4464.4	4570.7	23.6

Table 3: Evaluation of text-to-image generation capabilities.

Method	General Captions			Complex Prompts - Reasoning			
	CLIP-Score	FID (↓)	Inception Score	DrawBench Image Quality	DrawBench Caption Following	LIMA-test Image Quality	LIMA-test Instruction Following
Baseline (SDXL)	31.52	38.05	32.79	7.23	6.63	7.50	5.54
LLMGA-7B	–	–	–	6.98	5.69	7.35	5.56
Mini-Gemini-7B	31.29	37.67	33.11	7.48	6.98	8.33	7.60

High Resolution. To validate the framework for extended visual tokens, we perform experiments with an input size of 672 for LR visual encoder and 1536 for HR visual encoder in Table 1. As discussed above, the HR visual encoder primarily serves to offer high-resolution candidate information. Importantly, despite the increased resolution, *the effective number of visual tokens processed by the LLM remains consistent with the LR input size of 672*, ensuring computational efficiency. The benefits of this approach are particularly evident in detail-oriented tasks. For example, in the TextVQA Singh et al. (2019) benchmark, our method achieved a performance rate of 74.1% with the Hermes-2-Yi-34B configuration, closely matching the performance of the well-established Gemini Pro Team et al. (2023). Detailed results in Table 1 show that Mini-Gemini excels in more challenging benchmarks as well. For instance, the proposed method is on par with Qwen-VL-Plus Bai et al. (2023) on the MathVista Lu et al. (2024) and MMMU Yue et al. (2024) benchmark and even surpasses Gemini Pro and GPT-4V on the widely-adopted MMB Liu et al. (2023c) benchmark.

Computation Cost We report the component-wise inference time of the LLaVA-Wild benchmark in Table 2. As the cross attentions in path info mining with HR and LR features are mainly performed within the local region features with width $M = 8$, this parallel operation ensures that each LR query only attends to the local HR key and value with $8 \times 8 = 64$ features, which greatly reduces the cost. It does not bring much computational overhead in experiments. Due to the variable output token length affecting the inference speed of LLM, we also report the TFLOPs of generating the first 100 tokens in Table 2.

Reasoning Generation In Table 3, we set up a benchmark to evaluate the capability of text-to-image (T2I) generation from two aspects: (1) *T2I on general captions*. We used COCO Karpathy test captions to evaluate our method, reporting CLIP-Score, FID, and Inception-Score. Results indicate our method maintains performance consistent with SDXL on simple T2I tasks. (2) *Complex prompt T2I and reasoning generation*. We employed GPT-4o as an evaluator, scoring generated images from 1-10 in two aspects, image quality and instruction following, based on corresponding user inputs. We used LIMA-test Zhou et al. (2024) and DrawBench Saharia et al. (2022) as test sets. Results demonstrate our method’s superiority in understanding complex queries than Xia et al. (2023); Podell et al. (2023), producing more aesthetically pleasing and instruction-compliant images.

4.3 COMPONENT-WISE ANALYSIS

Patch Info Mining. We first delve into the proposed patch info mining and report results in Table 4. It is clear that the model achieves significant gains with the ConvNeXt-L integrated as the vision encoder for HR images. For example, when the LR and HR are respectively set to 224 and 512, the model increases 4.0% and 18.1 in TextVQA and MME datasets. Elevating the HR resolution to 768 further widens the performance margin, achieving a 5.7% uplift in TextVQA compared to the baseline. These results underscore the substantial impact of patch info mining in harnessing more detailed visual cues. When we further extend the LR resolution to 336, patch info mining still contributes consistent gains. For instance, with the default ConvNeXt-L as vision encoder, it surpasses the baseline with 3.3%, 6.3, and 3.5% in TextVQA Singh et al. (2019), MME Fu et al. (2023), and MM-Vet Yu et al. (2023) dataset, respectively. This proves the capability of designed modules with input resolution scaled up.

Table 4: Comparison with different info mining settings. The baseline is LLaVA-1.5 Liu et al. (2023a) with Vicuna-7B using the same training data and strategy. Token Num indicates the number of visual tokens T_V in Equation 1. * denotes that images in the *train* subset are included. Results with patch info mining are marked in . We respectively set ConvNeXt-L, 336, and 768 for HR Vision Encoder (VE-HR), LR image resolution (LR), and HR image resolution (HR) by default.

Method	VE-HR	LR	HR	Token Num.	VQA ^T		MME		MM-Vet	
Baseline	–	224	–	256	54.1*		1467.1		30.7	
+ Info mining	ConvX-L	224	512	256	58.1*	+4.0 	1485.2	+18.1 	31.3	+0.6
+ Higher res.	ConvX-L	224	768	256	59.8*	+1.7 	1478.3	-6.9 	31.9	+0.6
Baseline	–	336	–	576	58.2*		1510.7		31.1	
+ Info mining	ConvX-B	336	768	576	58.4*	+0.2 	1451.7	-59.0 	33.8	+2.7
+ Larger VE-HR	ConvX-L	336	768	576	61.5*	+3.1 	1517.0	+65.3 	34.6	+0.8
+ Larger VE-HR	ConvX-XXL	336	768	576	62.0*	+0.5 	1505.7	-11.3 	33.8	-0.8

Table 5: Comparison with different models and data settings. We take LLaVA-1.5 Liu et al. (2023a) with Vicuna-7B as our baseline. Token Num indicates the number of visual tokens T_V in Equation 1. * denotes images in *train* subset are included. Ablation studies on model and data are marked with and .

Method	LR	HR	Token Num.	VQA ^T		MME		MM-Vet	
Baseline	336	–	576	58.2*		1510.7		31.1	
+ Info mining	336	768	576	61.5*	+3.3 	1517.0	+6.3 	34.6	+3.5
+ ShareGPT4V	336	768	576	63.2*	+1.7 	1527.6	+10.6 	34.2	-0.4
- TextCaps	336	768	576	59.0	-4.2 	1465.2	-62.4 	35.0	+0.8
+ LAION-GPT-4V	336	768	576	58.7	-0.3 	1521.8	+56.6 	33.4	-1.6
+ OCR-related	336	768	576	61.6	+2.9 	1523.5	+1.7 	33.7	+0.3
+ Gen-related	336	768	576	62.2	+0.6 	1521.2	-2.3 	37.0	+3.3
+ ALLaVA	336	768	576	65.2	+3.0 	1523.3	+2.1 	40.8	+3.8
+ Token extension	672	1536	2880	68.4	+3.2 	1546.2	+22.9 	41.3	+0.5

Vision Encoder. To investigate the effect brought by mining candidates, we conduct experiments with various HR vision encoders in Table 4. Compared with the default ConvNeXt-L, we add two encoders for contrast trials, *i.e.*, ConvNeXt-B, and ConvNeXt-XXL. With ConvNeXt-B, the model performs better in TextVQA Singh et al. (2019) and MM-Vet Yu et al. (2023). However, the ConvNeXt-L encoder consistently delivers peak results, especially in the MME and MM-Vet datasets, indicating a superior balance in handling detailed visual information. We can conclude from the table that a larger vision encoder for HR images contributes more to the candidate quality, but the model converges with an extremely large encoder like ConvNeXt-XXL. Hence, considering the balance between effectiveness and computational efficiency, ConvNeXt-L is chosen as the default HR vision encoder. This decision is based on its ability to provide high-quality visual information mining while maintaining reasonable computational demands, as evidenced by the comparative performance across the benchmarks.

High-quality Data. In this era, the significance of high-quality data for enhancing the capabilities of LLMs and VLMs cannot be overstated. In our comprehensive analysis of data combination effects, presented in Table 5, we begin with a baseline model incorporating patch info mining. The integration of high-quality captions from ShareGPT4V Chen et al. (2023b) yields improved visual alignment and performance gains. We validate the zero-shot performance on the TextVQA Singh et al. (2019) benchmark, notably removing TextCaps Sidorov et al. (2020) data from the training set in line with previous studies Liu et al. (2024). This modification led to a notable performance decrease, underscoring the value of specific data types in training. To counteract this decline, we incorporate additional high-quality captions from LAION-GPT-4V eV and OCR-specific data, thus enhancing the model’s OCR reasoning capabilities. More details are provided in the appendix. As elaborated in Section 3.3, we utilize generation-related instructions to expand the application. It is interesting to find that such data also benefits the image understanding ability and brings 3.3% gains in MM-Vet dataset. Moreover, with the high-quality GPT4V responses from ALLaVA Chen et al. (2024) dataset, the framework respectively pushes the baseline over 7% and 9% in TextVQA and MM-Vet datasets. This comprehensive evaluation underscores the pivotal role of strategic high-quality data integration in amplifying the potential of the Mini-Gemini framework.

Visual Token Extension. As depicted in Figure 3b, the proposed patch info mining is adeptly designed to accommodate extended visual tokens, thereby generalizing its utility across different

432
433
434
435
436
437
438
439
440
441
442
443
444
445
446
447
448
449
450
451
452
453
454
455
456
457
458
459
460
461
462
463
464
465
466
467
468
469
470
471
472
473
474
475
476
477
478
479
480
481
482
483
484
485

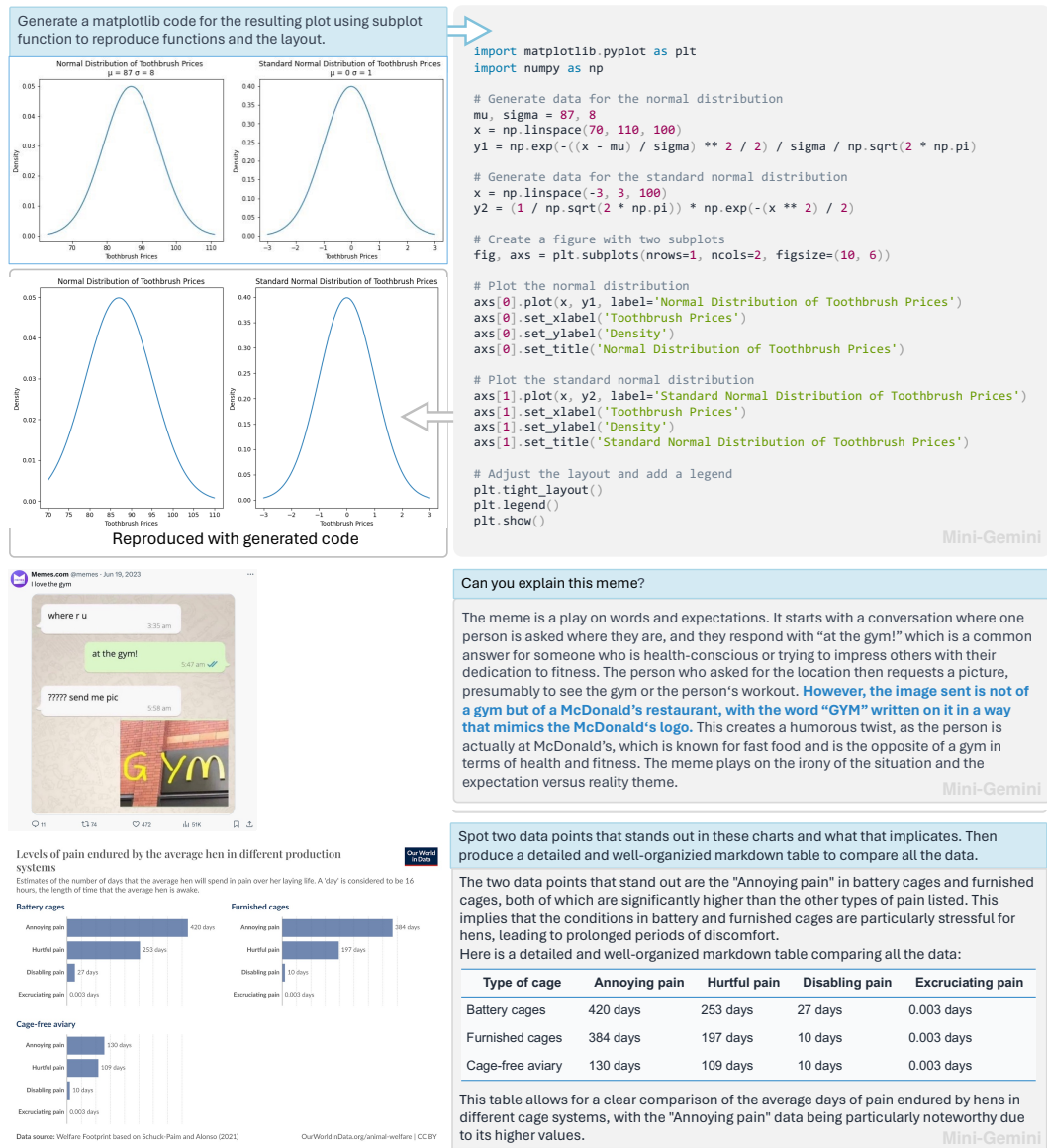


Figure 5: Qualitative results in visual understanding with Mini-Gemini.

input resolutions. We validate the effectiveness of the token extension in Table 5. When increasing LR and HR input resolution, the model achieves significant gain in all benchmarks. Notably, in detail-oriented tasks such as TextVQA, we observe a performance uplift of over 3%, indicating a significant enhancement in the model’s ability to handle complex visual data. Our empirical observations suggest that the increase in resolution significantly diminishes visual hallucinations, leading to more accurate and reliable image comprehension. Generally, with the increased visual token number, Mini-Gemini can be scaled up towards better capability.

4.4 QUALITATIVE RESULTS

Visual Understanding. To ascertain the visual comprehension prowess of Mini-Gemini in real-world settings, we apply it to a variety of understanding and reasoning tasks in Figure 5. Thanks to the patch info mining and high-quality data, Mini-Gemini can well solve several complex cases. For example, it is capable of recognizing plotted curves in graphical data and directly translating them into Python code for immediate application. Beyond mere recognition, it exhibits a keen attention to detail, demonstrating a nuanced understanding of character associations in memes. Moreover, Mini-Gemini’s analytical capabilities extend to chart analysis and practical problem-solving.

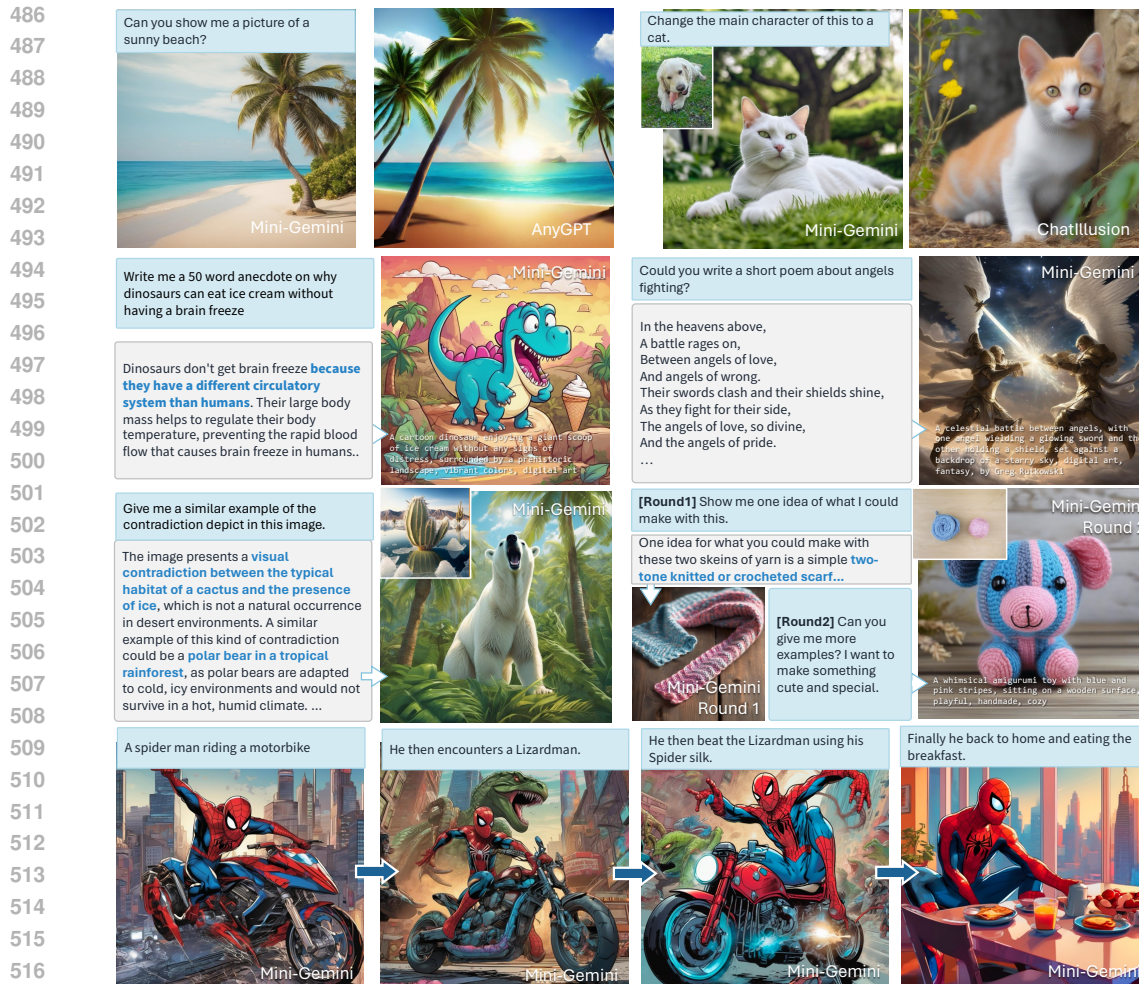


Figure 6: Qualitative results in image generation with Mini-Gemini.

Image Generation. In Figure 6, we provide a comprehensive evaluation of Mini-Gemini’s generation capabilities. Compared with recent studies such as AnyGPT Zhan et al. (2024) and ChatIllusion Chi et al. (2023), our stronger multi-modal understanding ability allows us to generate text-to-image captions that better align with the given instructions, resulting in more contextually appropriate image-text answers. A noteworthy point, as shown in Figures 1 and 6, is its proficiency in generating high-quality content based on multi-modal human instructions, with text-only training data. This capability underscores Mini-Gemini’s robust image-text alignment and semantic interpretation skills, which come into play effectively in the inference stage. Leveraging the VLM’s reasoning ability, Mini-Gemini produces coherent image-text outputs in various conversational scenarios.

5 CONCLUSION

We presented Mini-Gemini, a streamlined and potent framework for multi-modality VLMs. The essence of Mini-Gemini is to harness the latent capabilities of VLMs through strategic framework design, enriched data quality, and expanded functional scope. At its core, patch info mining enables efficient extraction of detailed visual cues by engaging with high-resolution candidates. From the data perspective, our meticulously compiled high-quality dataset ensures accurate vision-language alignment and bolsters strong instruction-following ability. Furthermore, we support reasoning-based generation in Mini-Gemini and empower current VLMs with image generation. Extensive experiments on several zero-shot benchmarks prove the superiority of the proposed method, which surpasses previous leading approaches and even private models. We hope the Mini-Gemini can serve as a strong benchmark for image understanding and VLM-guided generation.

REFERENCES

- 540
541
542 stable-diffusion-prompts. URL [https://www.gigasheet.com/sample-data/
543 stable-diffusion-prompts](https://www.gigasheet.com/sample-data/stable-diffusion-prompts). 5
- 544 Emanuele Aiello, Lili Yu, Yixin Nie, Armen Aghajanyan, and Barlas Oguz. Jointly training large
545 autoregressive multimodal models. *arXiv:2309.15564*, 2023. 5
- 546
547 Jean-Baptiste Alayrac, Jeff Donahue, Pauline Luc, Antoine Miech, Iain Barr, Yana Hasson, Karel
548 Lenc, Arthur Mensch, Katherine Millican, Malcolm Reynolds, et al. Flamingo: a visual language
549 model for few-shot learning. In *NeurIPS*, 2022. 3
- 550 Jinze Bai, Shuai Bai, Shusheng Yang, Shijie Wang, Sinan Tan, Peng Wang, Junyang Lin, Chang
551 Zhou, and Jingren Zhou. Qwen-vl: A frontier large vision-language model with versatile abilities.
552 *arXiv:2308.12966*, 2023. 2, 6, 7
- 553
554 Rohan Bavishi, Erich Elsen, Curtis Hawthorne, Maxwell Nye, Augustus Odena, Arushi Somani, and
555 Sağnak Taşlılar. Introducing our multimodal models, 2023. URL [https://www.adept.ai/
556 blog/fuyu-8b](https://www.adept.ai/blog/fuyu-8b). 2
- 557 James Betker, Gabriel Goh, Li Jing, Tim Brooks, Jianfeng Wang, Linjie Li, Long Ouyang, Juntang
558 Zhuang, Joyce Lee, Yufei Guo, et al. Improving image generation with better captions. *Computer
559 Science*. <https://cdn.openai.com/papers/dall-e-3.pdf>, 2(3):8, 2023. 3, 5
- 560
561 Tom Brown, Benjamin Mann, Nick Ryder, Melanie Subbiah, Jared D Kaplan, Prafulla Dhariwal,
562 Arvind Neelakantan, Pranav Shyam, Girish Sastry, Amanda Askell, et al. Language models are
563 few-shot learners. In *NeurIPS*, 2020. 2
- 564 Guiming Hardy Chen, Shunian Chen, Ruifei Zhang, Junying Chen, Xiangbo Wu, Zhiyi Zhang,
565 Zhihong Chen, Jianquan Li, Xiang Wan, and Benyou Wang. Allava: Harnessing gpt4v-synthesized
566 data for a lite vision-language model. *arXiv:2402.11684*, 2024. 2, 5, 8
- 567
568 Keqin Chen, Zhao Zhang, Weili Zeng, Richong Zhang, Feng Zhu, and Rui Zhao. Shikra: Unleashing
569 multimodal llm’s referential dialogue magic. *arXiv:2306.15195*, 2023a. 6
- 570 Lin Chen, Jisong Li, Xiaoyi Dong, Pan Zhang, Conghui He, Jiaqi Wang, Feng Zhao, and Dahua Lin.
571 Sharegpt4v: Improving large multi-modal models with better captions. *arXiv:2311.12793*, 2023b.
572 2, 5, 8
- 573
574 Xinlei Chen, Hao Fang, Tsung-Yi Lin, Ramakrishna Vedantam, Saurabh Gupta, Piotr Dollár,
575 and C Lawrence Zitnick. Microsoft coco captions: Data collection and evaluation server.
576 *arXiv:1504.00325*, 2015. 3
- 577 Xiaowei Chi, Yijiang Liu, Zhengkai Jiang, Rongyu Zhang, Ziyi Lin, Renrui Zhang, Peng Gao,
578 Chaoyou Fu, Shanghang Zhang, Qifeng Liu, et al. Chatillusion: Efficient-aligning interleaved
579 generation ability with visual instruction model. *arXiv preprint arXiv:2311.17963*, 2023. 3, 5, 10,
580 21
- 581 Wei-Lin Chiang, Zhuohan Li, Zi Lin, Ying Sheng, Zhanghao Wu, Hao Zhang, Lianmin Zheng,
582 Siyuan Zhuang, Yonghao Zhuang, Joseph E. Gonzalez, Ion Stoica, and Eric P. Xing. Vicuna:
583 An open-source chatbot impressing gpt-4 with 90%* chatgpt quality. [https://lmsys.org/
584 blog/2023-03-30-vicuna/](https://lmsys.org/blog/2023-03-30-vicuna/), 2023. 2
- 585
586 Xiangxiang Chu, Limeng Qiao, Xinyang Lin, Shuang Xu, Yang Yang, Yiming Hu, Fei Wei, Xinyu
587 Zhang, Bo Zhang, Xiaolin Wei, et al. Mobilevlm: A fast, reproducible and strong vision language
588 assistant for mobile devices. *arXiv:2312.16886*, 2023. 6
- 589 Wenliang Dai, Junnan Li, Dongxu Li, Anthony Meng Huat Tiong, Junqi Zhao, Weisheng Wang,
590 Boyang Li, Pascale Fung, and Steven Hoi. Instructblip: Towards general-purpose vision-language
591 models with instruction tuning. *arXiv:2305.06500*, 2023. 2, 3, 4, 6
- 592
593 Jacob Devlin, Ming-Wei Chang, Kenton Lee, and Kristina Toutanova. Bert: Pre-training of deep
bidirectional transformers for language understanding. *arXiv:1810.04805*, 2018. 2

- 594 Xiaoyi Dong, Pan Zhang, Yuhang Zang, Yuhang Cao, Bin Wang, Linke Ouyang, Xilin Wei, Songyang
595 Zhang, Haodong Duan, Maosong Cao, Wenwei Zhang, Yining Li, Hang Yan, Yang Gao, Xinyue
596 Zhang, Wei Li, Jingwen Li, Kai Chen, Conghui He, Xingcheng Zhang, Yu Qiao, Dahua Lin, and Ji-
597 aqi Wang. Internlm-xcomposer2: Mastering free-form text-image composition and comprehension
598 in vision-language large model. *arXiv preprint arXiv:2401.16420*, 2024. 3
- 599
600 LAION eV. Laion/gpt4v-dataset · datasets at hugging face. URL [https://huggingface.co/
601 datasets/laion/gpt4v-dataset](https://huggingface.co/datasets/laion/gpt4v-dataset). 5, 8
- 602 Chaoyou Fu, Peixian Chen, Yunhang Shen, Yulei Qin, Mengdan Zhang, Xu Lin, Zhenyu Qiu, Wei Lin,
603 Jinrui Yang, Xiawu Zheng, et al. Mme: A comprehensive evaluation benchmark for multimodal
604 large language models. *arXiv:2306.13394*, 2023. 6, 7
- 605
606 Yuying Ge, Yixiao Ge, Ziyun Zeng, Xintao Wang, and Ying Shan. Planting a seed of vision in large
607 language model. *arXiv preprint arXiv:2307.08041*, 2023a. 3
- 608 Yuying Ge, Sijie Zhao, Ziyun Zeng, Yixiao Ge, Chen Li, Xintao Wang, and Ying Shan. Making
609 llama see and draw with seed tokenizer. *arXiv preprint arXiv:2310.01218*, 2023b. 3
- 610
611 Google. Gemma: Introducing new state-of-the-art open models. [https://blog.google/
612 technology/developers/gemma-open-models/](https://blog.google/technology/developers/gemma-open-models/), 2024. 3, 6
- 613
614 Yash Goyal, Tejas Khot, Douglas Summers-Stay, Dhruv Batra, and Devi Parikh. Making the v in vqa
615 matter: Elevating the role of image understanding in visual question answering. In *CVPR*, 2017. 2,
616 3
- 617 Tianrui Guan, Fuxiao Liu, Xiyang Wu, Ruiqi Xian, Zongxia Li, Xiaoyu Liu, Xijun Wang, Lichang
618 Chen, Furong Huang, Yaser Yacoob, et al. Hallusionbench: an advanced diagnostic suite for
619 entangled language hallucination and visual illusion in large vision-language models. In *CVPR*, pp.
620 14375–14385, 2024. 16
- 621
622 IDEFICS. Introducing idefics: An open reproduction of state-of-the-art visual language model.
623 <https://huggingface.co/blog/idefics>, 2023. 6
- 624 Albert Q Jiang, Alexandre Sablayrolles, Antoine Roux, Arthur Mensch, Blanche Savary, Chris
625 Bamford, Devendra Singh Chaplot, Diego de las Casas, Emma Bou Hanna, Florian Bressand, et al.
626 Mixtral of experts. *arXiv:2401.04088*, 2024. 2, 3
- 627
628 Kushal Kafle, Brian Price, Scott Cohen, and Christopher Kanan. Dvqa: Understanding data visualiza-
629 tions via question answering. In *CVPR*, 2018. 5
- 630 Aniruddha Kembhavi, Mike Salvato, Eric Kolve, Minjoon Seo, Hannaneh Hajishirzi, and Ali Farhadi.
631 A diagram is worth a dozen images. In *ECCV*, 2016. 2, 5, 16
- 632
633 Andreas Köpf, Yannic Kilcher, Dimitri von Rütte, Sotiris Anagnostidis, Zhi Rui Tam, Keith
634 Stevens, Abdullah Barhoum, Duc Nguyen, Oliver Stanley, Richárd Nagyfi, et al. Openassistant
635 conversations-democratizing large language model alignment. *Advances in Neural Information
636 Processing Systems*, 36, 2024. 2, 5
- 637
638 Xin Lai, Zhuotao Tian, Yukang Chen, Yanwei Li, Yuhui Yuan, Shu Liu, and Jiaya Jia. Lisa: Reasoning
639 segmentation via large language model. *arXiv:2308.00692*, 2023. 3
- 640
641 Bo Li, Peiyuan Zhang, Jingkang Yang, Yuanhan Zhang, Fanyi Pu, and Ziwei Liu. Otterhd: A
642 high-resolution multi-modality model. *arXiv:2311.04219*, 2023a. 2, 6
- 643
644 Bohao Li, Rui Wang, Guangzhi Wang, Yuying Ge, Yixiao Ge, and Ying Shan. Seed-bench: Bench-
645 marking multimodal llms with generative comprehension. *arXiv preprint arXiv:2307.16125*, 2023b.
646 16
- 647
648 Junnan Li, Dongxu Li, Silvio Savarese, and Steven Hoi. Blip-2: Bootstrapping language-image
649 pre-training with frozen image encoders and large language models. *arXiv:2301.12597*, 2023c. 1,
650 3

- 648 Yanwei Li, Chengyao Wang, and Jiaya Jia. Llama-vid: An image is worth 2 tokens in large language
649 models. *arXiv:2311.17043*, 2023d. **1, 6**
650
- 651 Yifan Li, Yifan Du, Kun Zhou, Jinpeng Wang, Wayne Xin Zhao, and Ji-Rong Wen. Evaluating object
652 hallucination in large vision-language models. *arXiv preprint arXiv:2305.10355*, 2023e. **16**
653
- 654 Ziyi Lin, Chris Liu, Renrui Zhang, Peng Gao, Longtian Qiu, Han Xiao, Han Qiu, Chen Lin, Wenqi
655 Shao, Keqin Chen, et al. Sphinx: The joint mixing of weights, tasks, and visual embeddings for
656 multi-modal large language models. *arXiv:2311.07575*, 2023. **2**
- 657 Haotian Liu, Chunyuan Li, Yuheng Li, and Yong Jae Lee. Improved baselines with visual instruction
658 tuning. *arXiv:2310.03744*, 2023a. **3, 5, 6, 8**
659
- 660 Haotian Liu, Chunyuan Li, Qingyang Wu, and Yong Jae Lee. Visual instruction tuning. In *NerulPS*,
661 2023b. **1, 2, 3, 4**
- 662 Haotian Liu, Chunyuan Li, Yuheng Li, Bo Li, Yuanhan Zhang, Sheng Shen, and Yong Jae Lee.
663 Llava-next: Improved reasoning, ocr, and world knowledge, 2024. URL [https://llava-vl.
664 github.io/blog/2024-01-30-llava-next/](https://llava-vl.github.io/blog/2024-01-30-llava-next/). **2, 5, 6, 8**
665
- 666 Yuan Liu, Haodong Duan, Yuanhan Zhang, Bo Li, Songyang Zhang, Wangbo Zhao, Yike Yuan, Jiaqi
667 Wang, Conghui He, Ziwei Liu, et al. Mmbench: Is your multi-modal model an all-around player?
668 *arXiv:2307.06281*, 2023c. **2, 6, 7**
- 669 Yuliang Liu, Zhang Li, Biao Yang, Chunyuan Li, Xucheng Yin, Cheng-lin Liu, Lianwen Jin,
670 and Xiang Bai. On the hidden mystery of ocr in large multimodal models. *arXiv preprint
671 arXiv:2305.07895*, 2023d. **16**
672
- 673 Zhuang Liu, Hanzi Mao, Chao-Yuan Wu, Christoph Feichtenhofer, Trevor Darrell, and Saining Xie.
674 A convnet for the 2020s. In *CVPR*, 2022. **4**
- 675 Pan Lu, Swaroop Mishra, Tanglin Xia, Liang Qiu, Kai-Wei Chang, Song-Chun Zhu, Oyvind Tafjord,
676 Peter Clark, and Ashwin Kalyan. Learn to explain: Multimodal reasoning via thought chains for
677 science question answering. In *NeurIPS*, 2022. **3**
678
- 679 Pan Lu, Hritik Bansal, Tony Xia, Jiacheng Liu, Chunyuan Li, Hannaneh Hajishirzi, Hao Cheng,
680 Kai-Wei Chang, Michel Galley, and Jianfeng Gao. Mathvista: Evaluating mathematical reasoning
681 of foundation models in visual contexts. In *ICLR*, 2024. **6, 7**
- 682 Ahmed Masry, Do Xuan Long, Jia Qing Tan, Shafiq Joty, and Enamul Hoque. Chartqa: A benchmark
683 for question answering about charts with visual and logical reasoning. *arXiv:2203.10244*, 2022. **2,
684 5, 16**
685
- 686 Minesh Mathew, Dimosthenis Karatzas, and CV Jawahar. Docvqa: A dataset for vqa on document
687 images. In *Proceedings of the IEEE/CVF winter conference on applications of computer vision*,
688 pp. 2200–2209, 2021. **16**
- 689 OpenAI. Video generation models as world simulators. URL [https://openai.com/
690 research/video-generation-models-as-world-simulators](https://openai.com/research/video-generation-models-as-world-simulators). **5**
691
- 692 OpenAI. Chatgpt. <https://openai.com/blog/chatgpt/>, 2023a. **1, 2**
693
- 694 OpenAI. Gpt-4 technical report. *arXiv:2303.08774*, 2023b. **1, 2, 6**
695
- 696 Long Ouyang, Jeffrey Wu, Xu Jiang, Diogo Almeida, Carroll Wainwright, Pamela Mishkin, Chong
697 Zhang, Sandhini Agarwal, Katarina Slama, Alex Ray, et al. Training language models to follow
instructions with human feedback. In *NeurIPS*, 2022. **2**
- 698 PaddleOCR. Awesome multilingual ocr toolkits based on paddlepaddle. URL [https://github.
699 com/PaddlePaddle/PaddleOCR](https://github.com/PaddlePaddle/PaddleOCR). **16**
700
- 701 Pablo Pernias, Dominic Rampas, Mats L. Richter, Christopher J. Pal, and Marc Aubreville. Wuer-
stchen: An efficient architecture for large-scale text-to-image diffusion models, 2023. **5**

- 702 Dustin Podell, Zion English, Kyle Lacey, Andreas Blattmann, Tim Dockhorn, Jonas Müller, Joe
703 Penna, and Robin Rombach. Sdxl: Improving latent diffusion models for high-resolution image
704 synthesis. *arXiv preprint arXiv:2307.01952*, 2023. 2, 3, 5, 7
- 705
- 706 Alec Radford, Jong Wook Kim, Chris Hallacy, Aditya Ramesh, Gabriel Goh, Sandhini Agarwal,
707 Girish Sastry, Amanda Askell, Pamela Mishkin, Jack Clark, et al. Learning transferable visual
708 models from natural language supervision. In *ICML*, 2021. 3, 4, 5
- 709
- 710 Chitwan Saharia, William Chan, Saurabh Saxena, Lala Li, Jay Whang, Emily L Denton, Kamyar
711 Ghasemipour, Raphael Gontijo Lopes, Burcu Karagol Ayan, Tim Salimans, et al. Photorealistic
712 text-to-image diffusion models with deep language understanding. *NeurIPS*, 35:36479–36494,
713 2022. 7
- 714
- 715 Christoph Schuhmann, Romain Beaumont, Richard Vencu, Cade W Gordon, Ross Wightman, Mehdi
716 Cherti, Theo Coombes, Aarush Katta, Clayton Mullis, Mitchell Wortsman, Patrick Schramowski,
717 Srivatsa R Kundurthy, Katherine Crowson, Ludwig Schmidt, Robert Kaczmarczyk, and Jenia
718 Jitsev. LAION-5b: An open large-scale dataset for training next generation image-text models. In
NeurIPS, 2022. 4, 5
- 719
- 720 Piyush Sharma, Nan Ding, Sebastian Goodman, and Radu Soricut. Conceptual captions: A cleaned,
721 hypernymed, image alt-text dataset for automatic image captioning. In *ACL*, 2018. 5
- 722
- 723 Oleksii Sidorov, Ronghang Hu, Marcus Rohrbach, and Amanpreet Singh. Textcaps: a dataset for
724 image captioning with reading comprehension. In *ECCV*, 2020. 5, 8
- 725
- 726 Amanpreet Singh, Vivek Natarajan, Meet Shah, Yu Jiang, Xinlei Chen, Dhruv Batra, Devi Parikh,
727 and Marcus Rohrbach. Towards vqa models that can read. In *CVPR*, 2019. 6, 7, 8, 16
- 728
- 729 Quan Sun, Yufeng Cui, Xiaosong Zhang, Fan Zhang, Qiying Yu, Zhengxiong Luo, Yueze Wang,
730 Yongming Rao, Jingjing Liu, Tiejun Huang, et al. Generative multimodal models are in-context
731 learners. *arXiv preprint arXiv:2312.13286*, 2023a. 3, 5
- 732
- 733 Quan Sun, Qiying Yu, Yufeng Cui, Fan Zhang, Xiaosong Zhang, Yueze Wang, Hongcheng Gao,
734 Jingjing Liu, Tiejun Huang, and Xinlong Wang. Generative pretraining in multimodality. *arXiv
735 preprint arXiv:2307.05222*, 2023b. 3
- 736
- 737 Rohan Taori, Ishaan Gulrajani, Tianyi Zhang, Yann Dubois, Xuechen Li, Carlos Guestrin, Percy
738 Liang, and Tatsunori B. Hashimoto. Stanford alpaca: An instruction-following llama model.
739 https://github.com/tatsu-lab/stanford_alpaca, 2023. 2
- 740
- 741 Gemini Team, Rohan Anil, Sebastian Borgeaud, Yonghui Wu, Jean-Baptiste Alayrac, Jiahui Yu, Radu
742 Soricut, Johan Schalkwyk, Andrew M Dai, Anja Hauth, et al. Gemini: a family of highly capable
743 multimodal models. *arXiv:2312.11805*, 2023. 1, 2, 6, 7
- 744
- 745 Rubèn Tito, Dimosthenis Karatzas, and Ernest Valveny. Document collection visual question
746 answering. In *ICDAR 2021*, 2021. 2, 5, 16
- 747
- 748 Hugo Touvron, Thibaut Lavril, Gautier Izacard, Xavier Martinet, Marie-Anne Lachaux, Timothée
749 Lacroix, Baptiste Rozière, Naman Goyal, Eric Hambro, Faisal Azhar, Aurelien Rodriguez, Armand
750 Joulin, Edouard Grave, and Guillaume Lample. Llama: Open and efficient foundation language
751 models. *arXiv:2302.13971*, 2023. 1, 2, 3
- 752
- 753 Ashish Vaswani, Noam Shazeer, Niki Parmar, Jakob Uszkoreit, Llion Jones, Aidan N Gomez, Łukasz
754 Kaiser, and Illia Polosukhin. Attention is all you need. In *NeurIPS*, 2017. 2
- 755
- 756 Weihan Wang, Qingsong Lv, Wenmeng Yu, Wenyi Hong, Ji Qi, Yan Wang, Junhui Ji, Zhuoyi
757 Yang, Lei Zhao, Xixuan Song, et al. Cogvlm: Visual expert for pretrained language models.
arXiv:2311.03079, 2023. 6
- 758
- 759 Jason Wei, Maarten Bosma, Vincent Y Zhao, Kelvin Guu, Adams Wei Yu, Brian Lester, Nan Du, An-
760 drew M Dai, and Quoc V Le. Finetuned language models are zero-shot learners. *arXiv:2109.01652*,
761 2021. 2

- 756 Chenfei Wu, Shengming Yin, Weizhen Qi, Xiaodong Wang, Zecheng Tang, and Nan Duan. Visual
757 chatgpt: Talking, drawing and editing with visual foundation models. *arXiv:2303.04671*, 2023a. **3**
758
- 759 Haoning Wu, Zicheng Zhang, Erli Zhang, Chaofeng Chen, Liang Liao, Annan Wang, Chunyi Li,
760 Wenxiu Sun, Qiong Yan, Guangtao Zhai, et al. Q-bench: A benchmark for general-purpose
761 foundation models on low-level vision. *arXiv preprint arXiv:2309.14181*, 2023b. **16**
- 762 Bin Xia, Shiyin Wang, Yingfan Tao, Yitong Wang, and Jiaya Jia. Llmga: Multimodal large language
763 model based generation assistant. *arXiv preprint arXiv:2311.16500*, 2023. **3, 5, 7, 21**
764
- 765 Rui Yang, Lin Song, Yanwei Li, Sijie Zhao, Yixiao Ge, Xiu Li, and Ying Shan. Gpt4tools: Teaching
766 large language model to use tools via self-instruction. *arXiv:2305.18752*, 2023. **3**
- 767 Weihao Yu, Zhengyuan Yang, Linjie Li, Jianfeng Wang, Kevin Lin, Zicheng Liu, Xinchao Wang,
768 and Lijuan Wang. Mm-vet: Evaluating large multimodal models for integrated capabilities.
769 *arXiv:2308.02490*, 2023. **6, 7, 8**
770
- 771 Xiang Yue, Yuansheng Ni, Kai Zhang, Tianyu Zheng, Ruoqi Liu, Ge Zhang, Samuel Stevens, Dongfu
772 Jiang, Weiming Ren, Yuxuan Sun, Cong Wei, Botao Yu, Ruibin Yuan, Renliang Sun, Ming Yin,
773 Boyuan Zheng, Zhenzhu Yang, Yibo Liu, Wenhao Huang, Huan Sun, Yu Su, and Wenhua Chen.
774 Mmmu: A massive multi-discipline multimodal understanding and reasoning benchmark for expert
775 agi. In *CVPR*, 2024. **2, 6, 7**
- 776 Jun Zhan, Junqi Dai, Jiasheng Ye, Yunhua Zhou, Dong Zhang, Zhigeng Liu, Xin Zhang, Ruibin Yuan,
777 Ge Zhang, Linyang Li, et al. Anygpt: Unified multimodal llm with discrete sequence modeling.
778 *arXiv preprint arXiv:2402.12226*, 2024. **3, 5, 10**
- 779 Hang Zhang, Xin Li, and Lidong Bing. Video-llama: An instruction-tuned audio-visual language
780 model for video understanding. *arXiv:2306.02858*, 2023a. **1**
781
- 782 Pan Zhang, Xiaoyi Dong, Bin Wang, Yuhang Cao, Chao Xu, Linke Ouyang, Zhiyuan Zhao, Shuangrui
783 Ding, Songyang Zhang, Haodong Duan, Wenwei Zhang, Hang Yan, Xinyue Zhang, Wei Li,
784 Jingwen Li, Kai Chen, Conghui He, Xingcheng Zhang, Yu Qiao, Dahua Lin, and Jiaqi Wang.
785 Internlm-xcomposer: A vision-language large model for advanced text-image comprehension and
786 composition. *arXiv preprint arXiv:2309.15112*, 2023b. **3**
- 787 Susan Zhang, Stephen Roller, Naman Goyal, Mikel Artetxe, Moya Chen, Shuohui Chen, Christopher
788 Dewan, Mona Diab, Xian Li, Xi Victoria Lin, et al. Opt: Open pre-trained transformer language
789 models. *arXiv:2205.01068*, 2022. **1, 2**
790
- 791 Chunting Zhou, Pengfei Liu, Puxin Xu, Srinivasan Iyer, Jiao Sun, Yuning Mao, Xuezhe Ma, Avia
792 Efrat, Ping Yu, Lili Yu, et al. Lima: Less is more for alignment. *Advances in Neural Information*
793 *Processing Systems*, 36, 2024. **2, 5, 7**
- 794 Deyao Zhu, Jun Chen, Xiaoqian Shen, Xiang Li, and Mohamed Elhoseiny. Minigpt-4: Enhancing
795 vision-language understanding with advanced large language models. *arXiv:2304.10592*, 2023. **1,**
796 **3**
797
798
799
800
801
802
803
804
805
806
807
808
809

A APPENDIX

B DATA COLLECTION DETAILS

Image-text Data Collection. In this section, we delve into the specifics of OCR-related data collection. Natural images can be easily annotated with detailed captions, but text-rich figures or diagrams, such as documents [Tito et al. \(2021\)](#), charts [Masry et al. \(2022\)](#), and scientific diagrams [Kembhavi et al. \(2016\)](#), present a more intricate challenge for models in complex questions and answers. Therefore, to facilitate the optimization process, we follow the strategy in TextVQA [Singh et al. \(2019\)](#) and incorporate OCR tokens for model reference in the training phase. In particular, we utilize the PaddleOCR [PaddleOCR](#) to initially identify and extract textual elements within each image. Then, we append the text characters to the original conversations in a format of `Reference OCR token:Text_1, ..., Text_n`, where `Text_1` to `Text_n` indicates n detected text strings. This approach ensures that the model has access to textual representations from the images, enhancing its ability to understand the image content. It is important to note that the OCR detector is utilized solely for generating enriched data and is not employed during testing. This distinction underscores our objective to train Mini-Gemini with a comprehensive understanding of both textual and visual elements, thereby improving capability in complex image-text scenarios.

Generation Data Collection. For the data generation collection described in Section 3.3, we provide specific examples of query prompts and their corresponding reference data sources for two generation tasks in Figure 7. We commence with a corpus comprising 10K GPT4V caption data and 6K English-only LLM SFT data. After filtering out results that did not meet the format requirements, we ultimately obtained 13K data points. To enhance the contextuality and quality of the queries, we incorporate two distinct types of in-context examples: `get_example_captions()` and `get_example_queries()`. The former function randomly selects 5 high-quality Stable Diffusion (SD) Text-to-Image (T2I) prompts, while the latter extracts 3 instances from a repository of simple instructional templates. These in-context examples serve as a foundational guide, providing diverse and representative prompts that significantly enrich the generation process. This strategic approach ensures the production of high-quality, relevant data, effectively supporting the generative capabilities.

C LIMITATIONS

Although Mini-Gemini achieves good results, it still has great potential to be further explored. For visual comprehension, the counting ability and complex visual reasoning ability are still far from satisfactory. This could be attributed to the lack of corresponding training data especially in the pretraining stage. Meanwhile, for reasoning-based generation, we use text to bridge the VLM and diffusion model in this work because we do not find apparent gain with embedding-based approaches. We will try to find a more advanced manner for visual understanding, reasoning, and generation.

D BROADER IMPACTS

The proposed method enhances Vision-Language Models (VLMs) for image understanding and generation. However, it is important to acknowledge that the current technique, while innovative, may not comprehensively address all possible scenarios in the short term. Given the complexity and variability of real-world visual data, there are potential risks of inaccuracies or errors in the generated responses. For instance, certain edge cases or highly context-specific queries might challenge the model’s current capabilities, leading to less reliable outcomes. This limitation underscores the need for continued research and development to improve the robustness and reliability of VLMs.

E RESULTS ON EXTRA BENCHMARKS.

We added experiments on 7 extra benchmarks for a comprehensive evaluation, including LLaVA-Wild, POPE [Li et al. \(2023e\)](#), SEED [Li et al. \(2023b\)](#), OCRBench [Liu et al. \(2023d\)](#), DocVQA [Mathew et al. \(2021\)](#), Q-Bench [Wu et al. \(2023b\)](#), and HallusionBench [Guan et al. \(2024\)](#). The results are

Table 6: Results on extra benchmarks. The results are reported with the same setting as in Table 1. * indicates the results evaluated using the official code.

Method	LLM	Res.	LLaVA-Wild	POPE	SEED	OCRBench	DocVQA	Q-Bench	HallusionBench
LLaVA-1.5	Vicuna-7B	336	63.4	85.9	58.6	31.6*	28.1*	58.7*	27.6*
LLaVA-1.5	Vicuna-13B	336	70.7	85.9	61.6	33.6*	30.3*	62.1*	24.5*
LLaVA-NeXT	Hermes-2-Yi-34B	672	89.6	87.7	75.9	57.2*	83.9*	71.8*	34.8
Mini-Gemini	Vicuna-7B	336	83.6	86.0	69.4	44.5	56.1	65.2	31.6
Mini-Gemini	Vicuna-13B	336	83.3	85.0	70.0	46.1	69.5	68.3	34.8
Mini-Gemini	Mixtral-8x7B	336	83.5	86.9	72.9	48.2	65.9	70.8	37.8
Mini-Gemini	Hermes-2-Yi-34B	336	89.4	86.0	73.8	48.6	67.1	72.0	43.7
Mini-Gemini-HD	Hermes-2-Yi-34B	672	91.2	87.7	75.5	59.1	84.2	74.6	41.5

summarized in Table 6. As presented in the table, our proposed method surpasses the typical VLMs (like LLaVA-1.5 and LLaVA-NeXT) on most benchmarks with different settings and resolutions. With Table 1, we show that Mini-Gemini surpasses LLaVA-NeXT on most benchmark evaluations (11 out of 14).

F EXTENDED SHOWCASES

In this section, we further provide more cases to validate the generality and capability of Mini-Gemini in various environments. As presented in Figures 8 and 9, Mini-Gemini can well answer detail-oriented questions and solve OCR-related and scientific problems. For image generation, we present more examples in Figure 10 that include direct T2I generation, multi-round conversation, reasoning-based generation, storytelling, and in-context generation. They further prove the superiority of Mini-Gemini in both visual comprehension and generation.

918
919
920
921
922
923
924
925
926
927
928
929
930
931
932
933
934
935
936
937
938
939
940
941
942
943
944
945
946
947
948
949
950
951
952
953
954
955
956
957
958
959
960
961
962
963
964
965
966
967
968
969
970
971

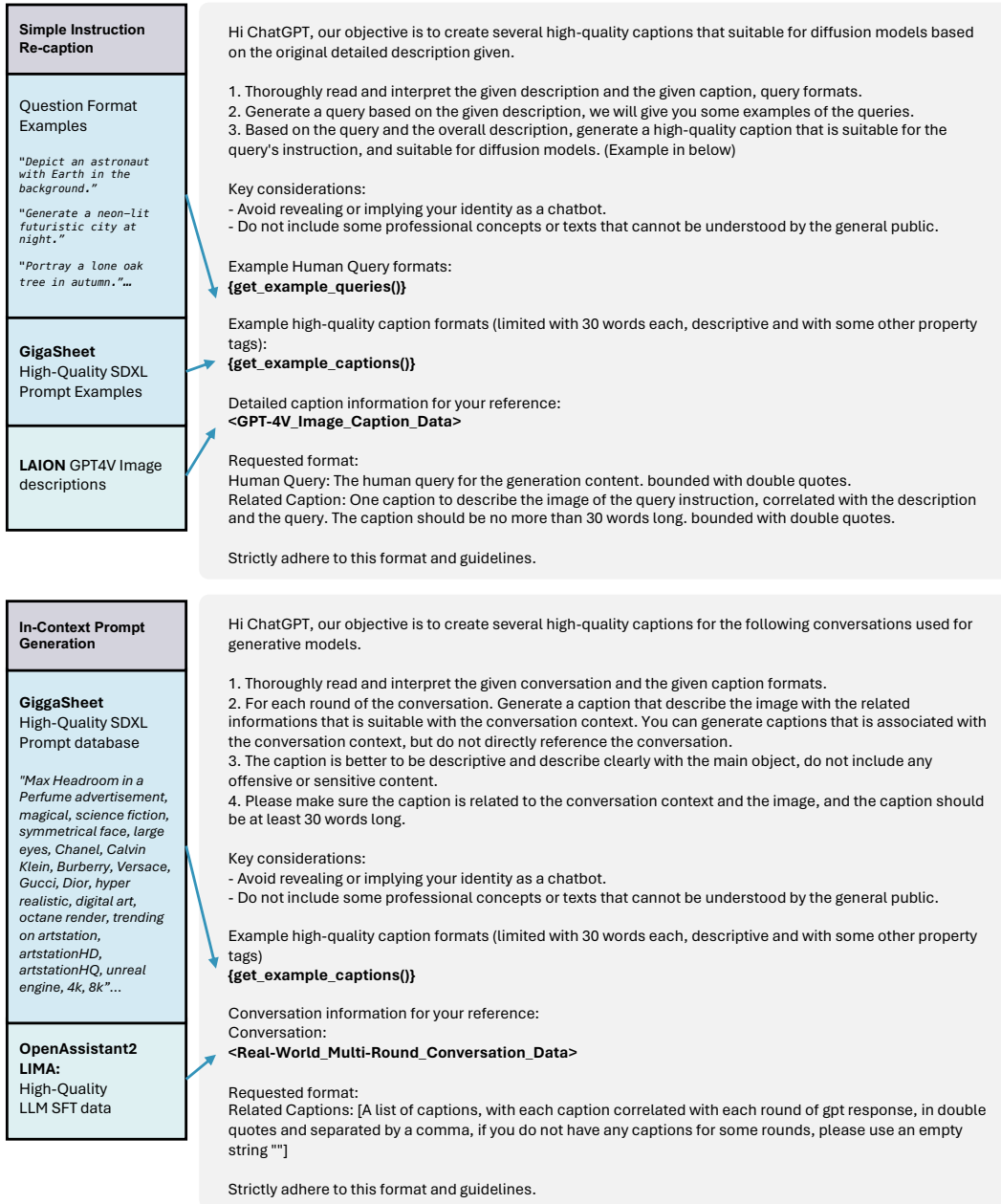



Figure 7: A detailed prompt design and data source illustration used for allocating image generation data. The total cost for the GPT-4 API to get all 13K data is around 80\$.

972
973
974
975
976
977
978
979
980
981
982
983
984
985
986
987
988
989
990
991
992
993
994
995
996
997
998
999
1000
1001
1002
1003
1004
1005
1006
1007
1008
1009
1010
1011
1012
1013
1014
1015
1016
1017
1018
1019
1020
1021
1022
1023
1024
1025




1

1. Can you explain this meme?

The meme uses a visual metaphor to represent the relationship between different programming languages and Chat-GPT, a language model developed by OpenAI. The tree trunk represents the foundational technologies that support web development, with Java and Python being two of the most popular programming languages. JavaScript and HTML are also essential technologies for web development, with JavaScript being the scripting language that adds interactivity to web pages and HTML being the markup language that defines the structure of web pages. The character labeled "Chat-GPT" is depicted as a lumberjack cutting down the tree, which symbolizes the disruptive impact that Chat-GPT could have on the traditional programming landscape. The meme humorously suggests that Chat-GPT might be so powerful or efficient that it could replace the need for these foundational technologies, much like a lumberjack cuts down a tree.

The meme plays on the idea that Chat-GPT, with its advanced natural language processing capabilities, could potentially simplify or automate tasks that were previously done by programmers using these languages. It's a lighthearted way to comment on the evolving nature of technology and the potential for new tools to change the way we work.

Mini-Gemini




2

2. Write HTML and CSS code to create a webpage based on the image shown. You should provide one .html file and one .css file.

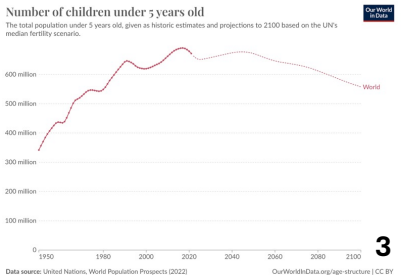
```

<!DOCTYPE html>
<html>
<head>
<title>Welcome!</title>
<link rel="stylesheet" type="text/css" href="style.css">
</head>
<body>
<h1>Welcome!</h1>
<p>This is a simple webpage.</p>
<ul>
<li><a href="#">Home</a></li>
<li><a href="#">About</a></li>
<li><a href="#">Contact</a></li>
</ul>
<button>Learn More</button>
<p>Contact us: <a href="mailto:email@example.com">email@example.com</a>
...
                    
```

render



Mini-Gemini

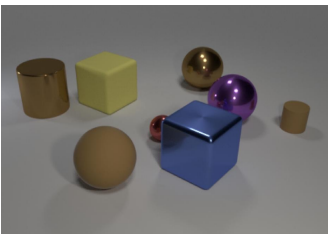


3

3. Describe this table in detail and summarize what you can get from this table.

The chart is a line graph that illustrates the historical and projected number of children under the age of 5 worldwide. The data is based on the United Nations' World Population Prospects from 2022. **The graph shows a general upward trend in the number of children under 5 from 1950 to around 2020, peaking at approximately 600 million. After 2020, the graph projects a decline in the number of children under 5, with the line descending towards the 400 million mark by 2100.** This suggests a projected decrease in the birth rate or an increase in the age at which women have children, leading to fewer children under 5 in the future. The graph is a useful tool for understanding demographic trends and can be used by policymakers, researchers, and organizations to plan for future needs, such as education and healthcare services for children.

Mini-Gemini




4


4. How many small spheres are the same color as the big rubber cube?

There are **no small spheres** that are the same color as the big rubber cube. **The big rubber cube is blue**, and there are no blue spheres present in the image.

Mini-Gemini



5



5. Please solve this issue. Tell me which option is the best choice.

The question appears to be a visual puzzle, likely from a logic or brain teaser book. The task is to identify which option (A, B, C, D, or E) is the best choice to replace the question mark in the sequence. To solve this, we need to look for a pattern or rule that applies to the sequence of shapes.

Upon inspection, **the sequence of shapes in the top row seems to be increasing in the number of sides: a triangle (3 sides), a square (4 sides), a pentagon (5 sides), and a hexagon (6 sides).** Following this pattern, the next shape should logically have seven sides, which is a heptagon.

Looking at the options provided, we can see that option A is a hexagon, which does not fit the pattern. Option B is a pentagon, which is a step back in the sequence. Option C is a triangle, which is too few sides. Option D is a heptagon, which fits the pattern of increasing sides. Option E is a hexagon, which does not fit the pattern.

Therefore, the best choice to replace the question mark in the sequence is option D, the heptagon, as it continues the pattern of increasing the number of sides on the shapes.

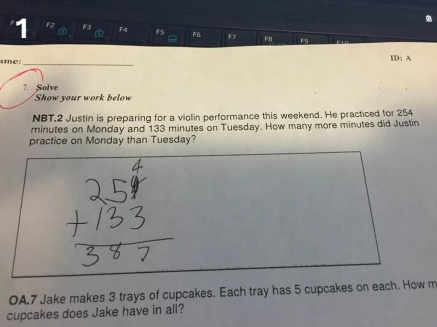
Mini-Gemini

Figure 8: Qualitative results of Mini-Gemini’s high-resolution understanding. We highlight a failed case in image understanding in orange.

19

1026
1027
1028
1029
1030
1031
1032
1033
1034
1035
1036
1037
1038
1039
1040
1041
1042
1043
1044
1045
1046
1047
1048
1049
1050
1051
1052
1053
1054
1055
1056
1057
1058
1059
1060
1061
1062
1063
1064
1065
1066
1067
1068
1069
1070
1071
1072
1073
1074
1075
1076
1077
1078
1079

1



1. Here's a solution to a Math problem by a student. Try to reason about the question step by step. Did the student get the correct answer?

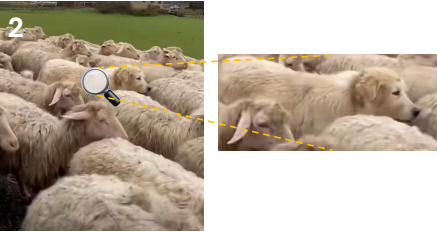
The student has attempted to solve the math problem by adding the number of minutes Justin practiced on Monday and Tuesday.

The student has correctly added 254 minutes (254 is 250 + 4) to 133 minutes, resulting in 387 minutes. However, the student has not accounted for the fact that Justin practiced more on Monday than on Tuesday.

The correct answer should be the difference between the total minutes Justin practiced on Monday and Tuesday, which is 254 minutes (Monday) - 133 minutes (Tuesday) = 121 minutes. Therefore, Justin practiced 121 more minutes on Monday than on Tuesday. The student's answer is incorrect as they have not subtracted the Tuesday practice time from the total Monday practice time.

Mini-Gemini

2




2. Why does this image look funny?

The image may appear funny **due to the unexpected and unusual sight of a dog seemingly 'hiding' among the sheep.** This is not a common occurrence, as dogs and sheep are distinct species with different behaviors and appearances. The dog's presence among the sheep, especially if it is a herding dog, can be seen as humorous because it contrasts with the typical expectation of a dog's role in a flock of sheep. Additionally, the dog's relaxed posture and the sheep's calm demeanor suggest a harmonious and comical coexistence, which can be amusing to observers. The image captures a moment that is both endearing and whimsical, which can elicit a light-hearted response from viewers.

Mini-Gemini

3

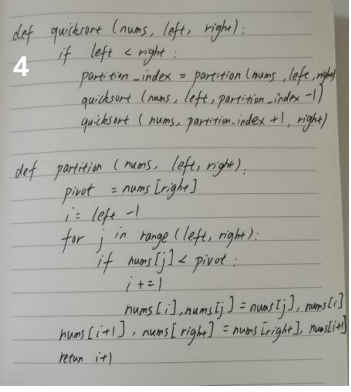


3. Choose one of the two pictures below to fill in the blank space above to maintain the pattern.

To maintain the pattern, the blank space above should be filled with the image of the green parrot. This is because the pattern alternates between the green parrot and the orange tiger, and since the last image in the sequence is the orange tiger, the next image should be the green parrot to continue the alternating pattern.

Mini-Gemini

4



4.a. Illustrate what problem this code in the image is addressing.

The code in the image is addressing the problem of sorting a list of numbers using the quicksort algorithm. Quicksort is a divide-and-conquer algorithm that works by selecting a pivot element from the list and partitioning the other elements into two sub-lists, according to whether they are less than or greater than the pivot. The partition function is used to find the index of the pivot element, which is then used to divide the list into two parts. The quicksort function then recursively sorts the two sub-lists, and the process continues until the entire list is sorted. This algorithm is efficient for large lists because it reduces the problem size by half with each recursive call.

Mini-Gemini

4.b. Transfer it to Python code here.


```
def quicksort(nums, left, right):
    if left < right:
        partition_index = partition(nums, left, right)
        quicksort(nums, left, partition_index - 1)
        quicksort(nums, partition_index + 1, right)

def partition(nums, left, right):
    pivot = nums[right]
    i = left - 1
    for j in range(left, right):
        if nums[j] < pivot:
            i += 1
            nums[i], nums[j] = nums[j], nums[i]
    nums[i + 1], nums[right] = nums[right], nums[i + 1]
    return i + 1
```

This code defines the quicksort function, which sorts a list of numbers by calling the partition function to find the index of the pivot element and then recursively sorting the two sub-lists. The partition function is used to partition the list into two parts, with elements less than the pivot on the left and elements greater than the pivot on the right. The pivot element is then placed in its correct position in the sorted list.

Mini-Gemini

5



Media saying AI will take over the world

My Neural Network

5. Explain this meme and illustrate what it implicates.

The meme is a humorous take on the common narrative that artificial intelligence (AI) will become so advanced that it will eventually surpass human capabilities and perhaps even take over the world. The left panel shows a person reacting with alarm, which is a common portrayal of the public's reaction to the idea of AI becoming too powerful. **The right panel, however, shows a cat labeled as a "Dog" by a neural network, which is a humorous example of AI making a mistake.** This juxtaposition implies that while AI is indeed becoming more advanced, it is not yet at the level where it can accurately perform tasks such as image recognition without errors. The meme uses this contrast to humorously downplay the fear of AI taking over, suggesting that the technology is still in its early stages and prone to mistakes.

Mini-Gemini

Figure 9: Qualitative results of Mini-Gemini's high-resolution understanding.

1080
1081
1082
1083
1084
1085
1086
1087
1088
1089
1090
1091
1092
1093
1094
1095
1096
1097
1098
1099
1100
1101
1102
1103
1104
1105
1106
1107
1108
1109
1110
1111
1112
1113
1114
1115
1116
1117
1118
1119
1120
1121
1122
1123
1124
1125
1126
1127
1128
1129
1130
1131
1132
1133



Figure 10: **Rows 1-2:** Comparison of Mini-Gemini with ChatIllusion Chi et al. (2023) and LLMGA Xia et al. (2023) on interactive image generation tasks. Mini-Gemini demonstrates superior adaptability and performance, capturing intricate details and maintaining coherence without further tuning on the text-image output alignment. **Rows 3-6** showcase Mini-Gemini’s unique capabilities in generating images with its plug-and-play capability, reasoning generation, and multi-round story-telling. All Mini-Gemini-generated images adopt SDXL unless otherwise specified.